Effects of bond relaxation on the martensitic transition and optical phonons in spontaneously ordered $GaInP_2$

A. M. Mintairov and J. L. Merz
Electrical Engineering Department, University of Notre Dame, Notre Dame, Indiana 46556

A. S. Vlasov
A.F. Ioffe Physical-Technical Institute, RAS, 26 Polytechnicheskaya, St. Petersburg 194021, Russia

(Received 30 January 2003; published 27 May 2003)

Strong changes of the Raman intensity induced by the martensitic transition in spontaneously ordered $GaInP_2$ alloys are explained by the triggering of the atom positions between unrelaxed (zinc-blende bond lengths) and relaxed ($CuPt_B$ bond lengths) arrangements. We show that these changes reflect a strong dependence of the optical-phonon properties and Raman selection rules of $CuPt_B$-ordered $GaInP_2$ on bond relaxation. Using analysis of the experimental spectra available in the literature we demonstrate that the relaxed and unrelaxed martensitic states can be detected by exciting different crystallographic planes. A strong effect of antiphase boundaries on the Raman spectra of spontaneously ordered $GaInP_2$ is revealed.

DOI: 10.1103/PhysRevB.67.205211 PACS number(s): 78.20.−e, 78.55.Cr, 63.20.−e, 78.30.Fs

I. INTRODUCTION

The $Ga_{0.5}In_{0.5}P$ alloy system presents a classic example of spontaneous atomic ordering in semiconductor alloys and was the subject of intense investigations of the influence of the ordering phenomena on structural and optical properties of semiconductors.[1–3] Growth of $Ga_{0.5}In_{0.5}P$ (hereafter referred to as $GaInP_2$) by metallo-organic vapor phase epitaxy on (001) GaAs substrates at temperatures near 650°C results in monolayer superlattice (MSL) alternation along the $\langle 111\rangle$ zinc-blende cubic diagonals. Of the four possible equivalent directions only two directions of the ordering ($[\bar{1}11]$ and $[1\bar{1}1]$, called $CuPt_B$ variants) have been observed in $GaInP_2$. Substrate orientations miscut several degrees towards the $[111]_B$ direction results in a single orientation of the ordered structure. The films grown under standard metalorganic vapor phase epitaxy (MOVPE) conditions are partially ordered, with an ordering parameter $\eta \sim 0.1-0.5$, where η is the fraction of the Ga(In) atoms in the $\{111\}_B$-GaP(InP) planes, or expressed equivalently, in the $\{111\}_B$-$Ga_{0.5(1+\eta)}In_{0.5(1-\eta)}P/Ga_{0.5(1-\eta)}In_{0.5(1+\eta)}P$ MSL. It was established that $CuPt_B$ ordering in $GaInP_2$ is promoted by surface reconstruction giving $[\bar{1}10]$ oriented surface dimers, and similar results have been observed for other III-V alloys, for growth conditions which provided such dimer orientations.[1,3]

In Ref. 4 we reported on the observation of a martensitic transition in the epitaxial layers of the single-variant $CuPt_B$-ordered $GaInP_2$. The martensitic transition is known in classical metallurgy as a diffusionless type-II phase transformation, associated only with rearrangement of lattice sites.[5] In the $GaInP_2$ the transition was detected using Raman spectroscopy and appeared as strong changes of intensity of the ordering-induced phonons after thermal treatment of the alloy film. It was shown that depending on the layer thickness and thermal treatment history there are at least two martensitic atomic arrangements (lattice states), which appear as two different intensity distributions of the optical phonons in $[-110]$ diagonal backscattering spectra excited from the growth (001) plane. Analysis of the Raman intensity using a bond polarizability model showed that these two states involve a rearrangement of the ordered lattice sites. However, the simplified version of the model, which accounts only for atom displacements of one sublattice, did not allow us to determine the nature of these states. While the origin of the martensitic states was not specified, a strong dependence of the spectra on layer thickness provides evidence that the driving force for the transition can be misfit strain arising from the symmetry difference between the substrate (zinc blende) and the $GaInP_2$ epitaxial layer (rhombohedral).

Our earlier observation implies that each $CuPt_B$-ordered $GaInP_2$ sample can be characterized by its matrensitic state, which can be established from the intensity distribution of the optical phonons in the Raman spectra. However, most of the experimental Raman data reported to date[6–22] do not account for this intrinsic lattice property of spontaneously ordered $GaInP_2$ and thus the analysis presented in these papers; which assumes a changing of the symmetry only, is not complete. The properties of the optical phonons of the $GaInP_2$ CuPt structure were also studied theoretically using microscopic lattice dynamical calculations for shell (unrelaxed[4]) and first-principles (relaxed[23,24]) models. A calculation of the directional dispersion using a bond charge model was also reported.[25] However, the open question about the origin of the martensitic states creates a level of uncertainty in comparing these theoretical results with experiment.

Raman studies of the effects of the $CuPt_B$ order on the optical phonons of the $GaInP_2$ have shown that in fully disordered samples ($\eta \sim 0$) there are two intense overlapping bands at 381 and 360 cm^{-1} related to longitudinal optical phonons LO_1 (GaP type) and LO_2 (InP type), respectively, and a weaker band at 330 cm^{-1} related to a transverse optical phonon TO_2 (InP type).[6,9–11] CuPt-type ordering for $\eta > 0$ induces the appearance of a new peak at 351 cm^{-1}, decreases the depth of the "valley" between the LO_1 and LO_2 bands at 370 cm^{-1}, and sharpens the TO_2 band. A new mode at 351 cm^{-1} was also observed in the IR spectra.[26–28]

Careful line-shape analysis reveals fine structure of optical-phonon bands.[4,28] Using different scattering geometries, involving polished $(\bar{1}\bar{1}1)$ and cleaved (110) planes, a rich set of data on the polarization properties of the optical phonon bands in spontaneously ordered $GaInP_2$ was obtained.[11–13] Inspection of the data given in this paper reveals several unusual observations of the Raman activity of the 351-cm^{-1} peak and the TO_2 band, which can be connected with different martensitic states. Our analysis allows us to assign a new 351-cm^{-1} mode to the vibration of the antiphase boundary.

In the present paper we analyze the Raman intensity of the $GaInP_2$ CuPt structure for the unrelaxed and relaxed lattice dynamical models. We used a complete version of the bond polarizability model for the $GaInP_2$ CuPt structure, which accounts for contributions of both sublattices.[29] Comparison of the selection rules obtained in this way with the experimental data allows us to connect the martensitic transition with relaxation of the bonds in the trigonal ternary $GaInP_2$ CuPt structure. We show that the transition can be described as a process involving lattice switching between relaxed (trigonal structure bond lengths) and unrelaxed (zinc-blende bond lengths) states of ordered domains governed by the symmetry misfit strains. This can be detected by Raman spectroscopy due to a strong dependence of the phonon properties of the $GaInP_2$ CuPt structure on the lattice relaxation, and due to specific selection rules which allow us to distinguish the modes of different sublattices. Using the experimental data available in the literature we demonstrate the possibility of detecting relaxed and unrelaxed martensitic states under excitation by means of different scattering planes, which gives evidence of mechanical treatment-induced triggering of the martensitic transition. We also reveal the strong effect of antiphase boundaries on the Raman spectra of the spontaneously ordered $GaInP_2$.

II. THE RAMAN SELECTION RULES FOR OPTICAL PHONONS OF CuPt-ORDERED $GaInP_2$

A. The effect of lattice relaxation on the optical phonons in CuPt ordered-$GaInP_2$

In a zinc-blende basis the principal axes of the perfectly ordered $CuPt_B$ structure having trigonal C_{3v}^5 space-group symmetry are z-$[111]$, y-$[11\bar{2}]$, and x-$[1\bar{1}0]$. Accommodation of different bond types in the ternary trigonal structure [Fig. 1(a)] leads to a distortion of the zinc-blende cubic cell along the [111] direction, providing anisotropic lattice mismatch along the [110] and $[\bar{1}10]$ directions [Fig. 1(b)]. The bond-length values obtained from the first-principles calculations[1,2,23,24] reveal frustration of Ga-P and compression of In-P bonds in perfectly ordered $GaInP_2$. This gives a mismatch of -1.5% for the $[\bar{1}10]$ direction and $+1.7\%$ for the [110] direction. For the unrelaxed structure (zinc-blende GaP and InP bond lengths) it is reduced down to $\sim 0.3\%$.

Having four basis atoms in the unit cell [inset in Fig. 1(a)], the $GaInP_2$ CuPt MSL therefore has 12 phonon branches. Nine fundamental zone-center optical modes are polar and active in both the Raman and IR spectra. Using a zone-folding scheme they can be grouped into three sets: an acoustic set and two optic sets of GaP- and InP-type modes, folded into the zone center from the acoustical and optical Brillouin zones boundary of the zinc-blende structure. Figures 2(a–c) present the angular dispersion of the folded optical-phonon frequencies of $GaInP_2$ CuPt calculated using the shell model with bulk bond lengths and interatomic potentials[4] [Fig. 2(a)] (unrelaxed model), the first-principles (relaxed) model[23,24] [Fig. 2(b)], and the spatial dispersion along the L direction of bulk zinc-blende GaP (Ref. 30) and InP (Ref 31) [Fig. 2(c)], together with the Raman experimental data from Refs. 4, 13, and 14 [in Figs. 2(a) and 2(b)].

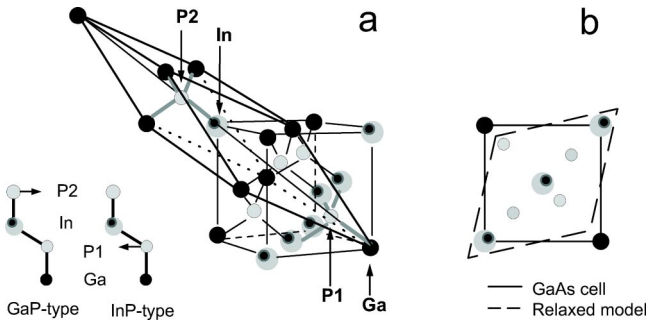

FIG. 1. (a) Rhombohedral symmetrical cell of the $GaInP_2$ $CuPt_B$-ordered structure together with GaP- and InP-type mode displacement patterns (inset in the left lower corner); (b) arrangement of atoms in zinc-blende (001) plane (dashed lines show distortion due to bond relaxation).

We can see from Figs. 2(a) and 2(b) that neglecting the type of the mode [inset[32] in Fig. 1(a)] as well as the difference in directional dispersion, two LO modes and one TO mode in both models occupy similar frequency regions centered at 370, 350, and 330 cm^{-1}, respectively. For the second TO mode the bond relaxation dramatically decreases the frequency (on 45 cm^{-1}) and moves it to the lowest-

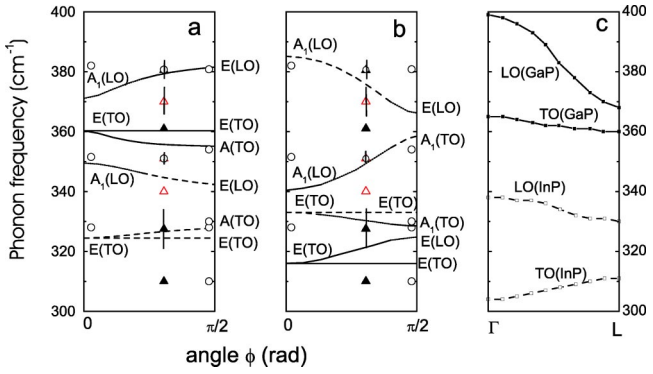

FIG. 2. Directional dispersion of $GaInP_2$ CuPt structure calculated in unrelaxed (Ref. 4) (a) and relaxed (Ref. 24) (b) models; spatial dispersion of bulk zinc-blende GaP and InP materials (Refs. 30 and 31)(c). Solid and dashed lines show vibrations of GaP and InP types, respectively, with dotted lines corresponding to the mixing region. Circles and triangles denote experimental data for main Raman peaks and for $\eta \sim 0.5$ from Ref. 13 and Refs. 4 and 14, respectively; solid symbols relate to modes observed for disordered samples and vertical lines scale half width of the mode in Raman spectra. The frequencies of the fine structure of these peaks revealed in Refs. 4 and 28 are not presented.

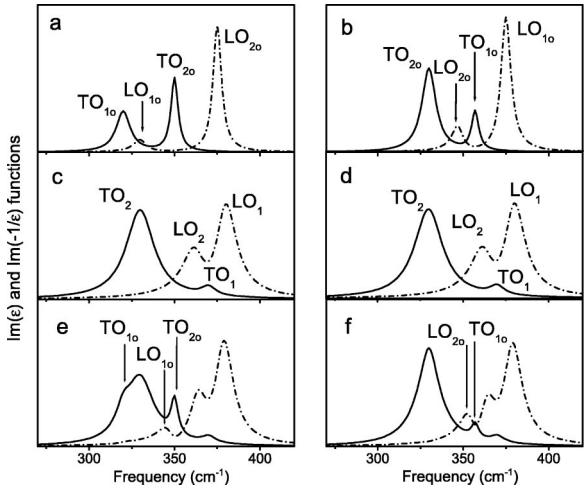

FIG. 3. Response functions $\mathrm{Im}(\varepsilon)$ for TO (solid curves) and $\mathrm{Im}(-\varepsilon^{-1})$ for LO (dashed-dotted curves) modes for perfectly ordered (a and b), disordered alloys (c and d) and partially ordered (e and f) $GaInP_2$ calculated for relaxed (a and e) and unrelaxed (b and f) models. Note that (c) and (d) are identical because disordered alloys are relaxed.

frequency position of $\sim 315\ \mathrm{cm}^{-1}$. Analysis of the phonon eigenmodes shows a greater difference between the models, which is the difference in the type (GaP or InP) of LO and TO mode alternation. In the shell model the frequencies are lower for the InP-type modes [dashed lines in Fig. 2(a)], while in the first-principles model the GaP-type ones have lower frequencies [solid lines in Fig. 2(b)]. In the first unrelaxed case the mode frequencies are close to the zone-edge frequencies of the bulk materials, i.e., they follow a simple zone-folding scheme in which material with heavier atoms (InP) has lower vibrational frequencies. In the second relaxed case, the decrease of the GaP-type and increase of the InP-type mode frequencies relative to the bulk values take place due to frustration and compression of the corresponding bonds.

From experimental phonon mode frequencies that have been presented in the literature, we can see that both models give reasonable agreement with the experiment, without distinguishing the mode type and accounting for the suppression of the anisotropy due to the mixed character of the ordering observed experimentally. This is demonstrated in Figs. 3(a–f), where we show transverse $\mathrm{Im}(\varepsilon)$ and longitudinal $\mathrm{Im}(-1/\varepsilon)$ phonon response functions for the ordered crystal (ε_o),[33] disordered alloy (ε_d),[34] and partially ordered alloy (ε_{po}).[35] For partially ordered alloy the functions have been calculated using the "η^2 rule":[36] $\varepsilon_{po}=\varepsilon_o\eta^2+\varepsilon_d(1-\eta^2)$. One can see clear differences in the intensity distribution of LO and TO modes in ordered and disordered crystals, arising from different LO/TO mode separations. For the ordered case [Figs. 3(a) and 3(b)], the low-frequency LO phonon has the lowest intensity mainly due to its position between two close transversal vibrations. This is different from the disordered alloy [Figs. 3(c) or 3(d)] in which the high-frequency TO mode has the lowest intensity due to its positioning between nearby LO modes. For $\eta \sim 0.5$ [Figs. 3(e) and 3(f)], both models give similar band shapes and qualitatively describe the appearance of an extra mode between the TO_2 and LO_2 bands of the disordered alloy together with a decrease of the valley depth at $370\ \mathrm{cm}^{-1}$ between disordered LO modes. The unrelaxed model also shows a sharpening of the TO_2 band at $330\ \mathrm{cm}^{-1}$, while in the relaxed model the sharpening is masked by a contribution of the ordered GaP-type TO_{1o} mode (shoulder at $\sim 320\ \mathrm{cm}^{-1}$). With a slight adjustment of the mode frequency and damping, both microscopic models can fit the IR reflectivity spectra of spontaneously ordered $GaInP_2$ measured in Ref. 26. However, the microscopic origin of the ordering-induced contribution is quite different. In the relaxed model the extra mode at $351\ \mathrm{cm}^{-1}$ is related to the TO_{2o} phonon (InP type), while in the unrelaxed model it can be either the LO_{2o} phonon (InP type) or the TO_{1o} phonon (GaP type); the depth of the valley at $370\ \mathrm{cm}^{-1}$ results from a contribution of the LO phonon of InP type for the relaxed model and of GaP-type for the unrelaxed one. Both GaP and InP modes contribute to the TO_2 band in the relaxed model while only the InP-type mode contributes in the unrelaxed one.

We should mention that the bond charge model also can describe the IR reflectivity spectra of spontaneously ordered $GaInP_2$.[25] It predicts extremely low angular anisotropy ($2-5\ \mathrm{cm}^{-1}$) compared with the unrelaxed ($5-10\ \mathrm{cm}^{-1}$) and relaxed ($10-20\ \mathrm{cm}^{-1}$) microscopic models. However, as the atom arrangement and the phonon eigenmodes were not specified, the relaxation of bonds and the type of the modes (InP or GaP) cannot be distinguished. We will not consider this model in further discusion.

B. The bond polarizability model Raman selection rules of CuPt-ordered $GaInP_2$

Compared to using the $\mathrm{Im}(\varepsilon)$ and $\mathrm{Im}(-1/\varepsilon)$ functions to determine the IR properties of the crystal, the Raman response functions contain additional contributions to mode intensities, which are determined by the symmetry of the lattice and by deformation potential and electro-optic mechanisms of the interaction of optical vibrations with light.[37] The first of these utilizes the Raman selection rules, which determine the relative intensity of a particular mode in different configurations. The second one utilizes the so-called Faust-Henry factors[38] which determine the relative intensity of the different modes in a single configuration. Both contributions can be treated simultaneously using the bond polarizability model.[39–41] This model accounts not only for the point symmetry but also for specific arrangements of atoms in the lattice. We will show that it allows one to distinguish between InP- and GaP-type modes, thus detecting the bond relaxation in $CuPt_B$. We will neglect the effect of the electro-optic contribution (related to LO phonons) in further consideration.

The bond polarizability model (BPM) of the Raman intensity is based on a transformation of the polarizability tensor of a single bond to the principal crystal axes, with a summation of the contributions of the nonequivalent bonds. If the alloy normal mode is localized in the ordered lattice sites, it will behave in the Raman spectra in a way similar to the normal modes of the perfectly ordered structure. In the

TABLE I. The Raman selection rules of $GaInP_2$ CuPt structure for geometries studied in the literature in notations of Fig. 4.

Wavevector	Configuration	Mode polarization			
		LO	TO[a]		Y'[b]
[001][c]	$Z(XX)\bar{Z}$	$3(1-\frac{4}{9}\Delta_\nu)^2$	$\frac{32}{27}\Delta_\nu$	0	$\frac{32}{27}\Delta_\nu$
	$Z(YY)\bar{Z}$	3	0	0	0
[110]	$y'(z'z')\bar{y'}$	0	$4(1-\Delta_\nu)^2$	0	$\frac{8}{3}(1-\Delta_\nu)^2$
	$y'(x'x')\bar{y'}$	0	1	2	$\frac{8}{3}$
	$y'(x'z')\bar{y'}$	0	0	1	$\frac{1}{3}$
$[\bar{1}11]$	$Z(XZ)X$	$2(1-\frac{2}{3}\Delta_\nu)^2$	1	0	$3(1-\frac{4}{9}\Delta_\nu)^2$
	$Z(YY)X$	1	2	0	0
	$Z(YZ)X$	0	0	3	0
	$Z(XY)X$	0	0	0	0
$[\bar{1}11]$	$z'(x'x')\bar{z'}$	1	2	0	2.7
	$z'(y'y')\bar{z'}$	1	2	0	0
	$z'(y'x')\bar{z'}$	0	0	2	0

[a]Right column corresponds to modes with polarization perpendicular to the (110) mirror plane (ordinary phonons).

[b]$[\bar{1}10]$ polarized mode.

[c]Wave vector does not coincide with the principal axes and the polarization of the modes may have arbitrary angle (extraordinary phonons). The selection rules for the extraordinary phonons are given by a linear combination of LO and TO contributions.

general case, the alloy normal modes involve the displacements of the bonds from both ordered and random atomic arrangements, which can be expressed in terms of coupling of the corresponding modes with selection rules averaged over all arrangements.

For the $GaInP_2$ CuPt structure the BPM tensors can be represented by the structure- (bond arrangement) dependent part multiplied by the mode displacement part, which is a sum of type-II (triple) bond displacements multiplied by the corresponding bond polarizability.[4] The structure-dependent part can be expressed as

$$\tilde{R}^z=\begin{pmatrix} -1 & 0 & 0 \\ 0 & -1 & 0 \\ 0 & 0 & 2(1-\Delta_\nu) \end{pmatrix},$$

$$\tilde{R}^y=\begin{pmatrix} \sqrt{2} & 0 & 0 \\ 0 & -\sqrt{2} & -1 \\ 0 & -1 & 0 \end{pmatrix}, \quad \tilde{R}^x=\begin{pmatrix} 0 & \sqrt{2} & -1 \\ \sqrt{2} & 0 & 0 \\ -1 & 0 & 0 \end{pmatrix}, \tag{1a}$$

$$\tilde{R}^{Y'}=\frac{1}{\sqrt{3}}\begin{pmatrix} 0 & 0 & 0 \\ 0 & -2\sqrt{2} & -1 \\ 0 & -1 & 2\sqrt{2}(1-\Delta_\nu) \end{pmatrix},$$

$$\tilde{R}^{Z'}=\frac{1}{\sqrt{3}}\begin{pmatrix} -3 & 0 & 0 \\ 0 & 1 & \sqrt{2} \\ 0 & \sqrt{2} & 2(1-\Delta_\nu) \end{pmatrix}, \tag{1b}$$

where $z\|[111]$, $y\|[11\bar{2}]$, $x\|[1\bar{1}0]$, $Y\|[110]$, and $Z\|[001]$. The tensors in Eq. (1b) are the Raman tensors for TO ($\tilde{R}^{Y'}$) and LO ($\tilde{R}^{Z'}$) modes for the [001] scattering wave vector (see below).

The tensors in Eq. (1a) have the same nonzero elements as those of the zinc-blende structure transformed to the trigonal basis. They have only one tensor element R^z_{zz}, which depends on the phonon eigenvector. This feature restricts possible Raman configurations sensitive to the properties of the specific phonons. The element R^z_{zz} can be expressed via a parameter Δ_ν, which reflects a trigonal distortion of the Raman polarizability of the zinc-blende structure for a given mode ν.[4,29] The rest of the elements have numerical values.

The value of Δ_ν can be obtained knowing the eigenvectors of the phonons and the bond polarizability values:[29]

$$\Delta_\nu=\frac{9}{8}\left[1-\frac{\alpha_1 U_1^I+\alpha_2 U_2^I}{\alpha_1 U_1^{\mathrm{II}}+\alpha_2 U_2^{\mathrm{II}}}\right]. \tag{2}$$

In Eq. (2) $U^{I(\mathrm{II})}_{1(2)}$ and $\alpha_{1(2)}$ are z components of the displacement and the polarizability derivative of the GaP- (InP-) type bond, respectively. In Ref. 42, the ratio α_2/α_1 was obtained to be ≈ 2.4.

The selection rules for four scattering conditions (geometries) accessible experimentally are listed in Table I. The arrangement of crystal axis and directions of light propagation and polarization for these four geometries are shown in Fig. 4. Three of these geometries involve growth planes (001) and cleaved planes (110). These are the backscattering geometries from the (001) and (110) planes having wave-

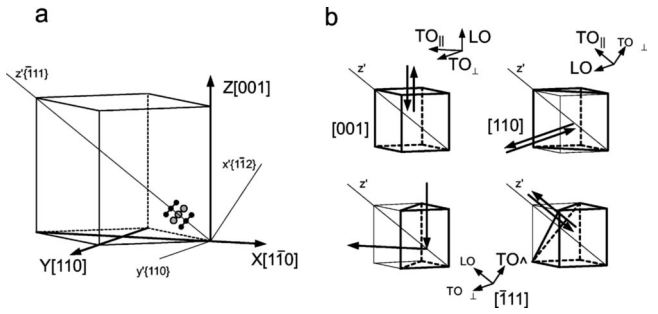

FIG. 4. Arrangement of the crystal axis of [$\bar{1}$11] oriented $CuPt_B$ structure, x',y',z', and directions of light polarizations, X,Y,Z (a), in notations of Ref. 11; schemes of [001] (upper left), [110] (upper right), [$\bar{1}$11] (lower right) backscattering and [$\bar{1}$11] right-angle scattering (lower left) Raman geometries (b). In (b) thick arrows show direction of light propagation and thin arrows shows phonon polarizations. The selection rules for this arrangement can be obtained using axis transformations $z\rightarrow z'$, $x\rightarrow y'$, and $y\rightarrow -x'$.

vector directions along [001] and [110], respectively, and the right-angle scattering geometry from these planes, having the wave vector along [$\bar{1}$11]. The fourth is the backscattering geometry from the ($\bar{1}$11) plane ([$\bar{1}$11] wave vector), which can obtained by mechanical polishing of the sample. In this paper we do not consider configurations involving the ($\bar{1}$10) cleaved plane because of the limited experimental data available[12]. We should point out that the selection rules in Table I are written for the ordering direction [$\bar{1}$11] and basis axes from Ref. 11

Only the geometries with the (001) and (110) scattering planes have configurations $Z(XZ)X$, $y'(z'z')\overline{y'}$, $Z(XX)\overline{Z}$ containing parameter Δ_ν. The comparison of the selection rules for these configurations with the reference ones, $Z(YY)X$, $y'(x'x')\overline{y'}$, $Z(YY)\overline{Z}$, which do not depend on Δ_ν and have the same scattering wave vector, allow determination of the contributions of the ordering-induced phonons.

As can be seen, the value and sign of Δ_ν determine the decrease or increase of the Raman intensity in the specific configuration. For pure GaP(InP) modes one can put $U^I_{1(2)} \ll U^{II}_{1(2)}$ (mode localization), thus simplifying this expression as $\Delta_{1(2)}=\frac{9}{8}[1-\alpha_{2(1)}/\alpha_{1(2)}]$. In this localized condition the trigonal distortion can be described independent of the phonon displacements, and the ordering-induced changes in the Raman intensity take place due to the difference in the bond polarizabilities of the two constituents. It has a different sign for GaP and InP-type modes, with the limiting values $\Delta_{InP}=+0.66$ and $\Delta_{GaP}=-1.58$ assuming $\alpha_2/\alpha_1\approx 2.4$.[42] Partial character of the ordering, i.e., mixing of the mode types, can be accounted for by a "η^2 rule,[36]" i.e., $U^I_{1(2)}=(1-\eta^2)U^{\rm II}_{1(2)}$, which leads to $\Delta_{\rm InP}=+0.125$ and $\Delta_{\rm GaP}=-0.14$.

In Table II we present the ratio of the Raman intensity of $Z(XZ)X$, $y'(z'z')\overline{y'}$, $Z(XX)\overline{Z}$ configurations to the reference ones calculated for these two conditions. We can see from Table II the dramatic effect of the localization compared with the mode mixing, which can lead to nearly an order of magnitude change of the Raman intensity. Due to the condition $\alpha_{InP}>\alpha_{\rm GaP}$ there is an increase of the GaP-type mode and decrease of the InP-type mode intensity due to the ordering. We should also mention the distinct selection rules for the Y' mode for [001] backscattering and [$\bar{1}$11] right-angle scattering geometries; it is activated only in the ordering-sensitive configurations $Z(XX)\overline{Z}$ and $Z(XZ)X$. For the [001] geometry this mode has TO polarization.

For the $Z(XX)\overline{Z}$ configuration both LO and TO phonons are ordering sensitive. For $\Delta_\nu\sim 0$ the Raman intensity in this configuration coincides with the reference one and thus any difference in their intensity can be directly related to the contribution of the ordering-induced phonons. We should stress that *only the vibrations of the ordered atomic arrangement give a contribution to the difference between* $Z(XX)\overline{Z}$ *and* $Z(YY)\overline{Z}$ *spectra*. This is a very important fact making these configurations very useful for identifying the ordering-induced phonons. The difference, which we called {110} anisotropy, is always positive ($I_{XX}\geqslant I_{YY}$) for TO phonons and for LO phonons of GaP type. For LO phonons of InP type it is negative. Thus the modes originating from the vibrations of different sublattices can be distinguished in the difference spectra. According to lattice dynamical analysis discussed, the bond relaxation shifts the InP-type LO phonon from $\sim$345 to $\sim$370 cm^{-1}. This must produce negative {110} anisotropy in the region of the LO_1 and LO_2 bands. In the unrelaxed state the negative anisotropy must appear below the LO_2 and near the TO_2 band.

TABLE II. Ordering-induced contributions in the Raman intensity of partially ordered $GaInP_2$ for mixed and localized modes.

Wave vector	Configuration	Mode polarization[a]					
		LO		TO		Y'	
		GaP	InP	GaP	InP	GaP	InP
[001]	$(XX)/(YY)$	1.1(3)	0.9(0.5)	∞	∞	∞	∞
[110]	$(z'z')/(x'x')$			1.7(9)	1(0.2)	1.3(7)	0.8(0.1)
[$\bar{1}$11]	$(XZ)/(YY)$	2.4(8)	1.7(0.6)	0.5[b]	0.5[b]	∞	∞

[a]Values for the localized modes are given in brackets.
[b]Does not depend on Δ_ν.

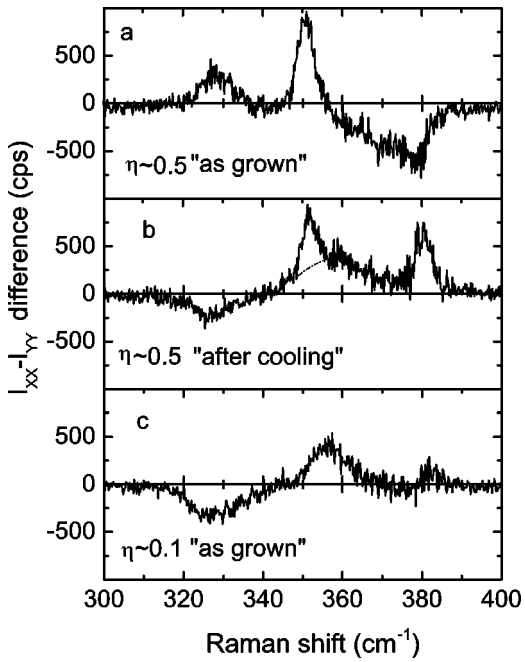

FIG. 5. $Z(XX)\bar{Z}/Z(YY)\bar{Z}$ difference spectra ([001] backscattering geometry) of 3-μm-thick spontaneously ordered $GaInP_2$ layers: (a) and (b) show highly ordered sample ($\eta\sim0.5$) before and after rapid cooling, respectively; (c) shows low ordered sample ($\eta\sim0.1$). Dashed line in (b) shows zero level (background) for the 351-cm^{-1} peak in $Z(XX)\bar{Z}$ configuration (Ref. 4).

For the [110] and $[\bar{1}11]$ wave-vector geometries, the determination of the ordering-induced contributions is not so transparent as the ratio of the mode intensity in the ordering-sensitive and reference configurations, for $\Delta_\nu=0$ is not equal to unity (4:1 for [110] and 2:1 for $[\bar{1}11]$ wave vectors).

Below we will compare the experimental Raman intensity data in the different scattering geometries reported in Refs. 4, 11, and 13 with the predictions of the BPM model, allowing us to determine the bond-relaxation origin of the martensitic transition in spontaneously ordered $GaInP_2$. This also reveals the contribution of the antiphase boundaries in the Raman spectra of these alloys.

III. PROPERTIES OF THE OPTICAL-PHONONS OF SPONTANEOUSLY ORDERED $GaInP_2$

A. Martensitic states in the Raman spectra of spontaneously ordered $GaInP_2$

1. Spectra for the wave vector [001]

The martensitic transition in the {110} anisotropy induced by $CuPt_B$ ordering in $GaInP_2$ is shown in Figs. 5(a) and 5(b). There we present difference between $Z(XX)\bar{Z}$ and $Z(YY)\bar{Z}$ spectra of a highly ordered ($\eta\sim0.5$) 3-μm-thick sample[4] before [Fig. 5(a)] and after [Fig. 5(b)] rapid cooling. In this figure we also show difference spectra of a low ordered ($\eta\sim0.1$) sample, which was not thermally treated [Fig. 5(c)].

Before transition the ordering-induced anisotropy is positive for the TO_2 band at 330 cm^{-1} and the 351-cm^{-1} peak and negative for the 360–380 cm^{-1} region (LO_2 and LO_1 bands and the ''valley depth''). This is exactly what is expected for the $CuPt_B$ bond relaxation of the ordered $GaInP_2$. The valley depth thus can be assigned as the ordering-induced LO_{2o} phonon (InP type) strongly mixed with the LO_1 and LO_2 modes of mostly disordered atomic arrangement. Such mixing produces the InP-type behavior of these modes. The anisotropy of the TO_2 band arises from the contributions of TO_{1o} and LO_{1o} phonons (of GaP type). The peak 351 cm^{-1} is activated only in the ordering-sensitive configuration and can be unambiguously assigned to the $[\bar{1}10]$ polarized mode. This coincides well with its interpretation as the TO_{2o} phonon (InP type) for the relaxed model. However, our analysis presented below does not allow the assignment of this peak as originating from the $CuPt_B$-type order. Instead it can be attributed to an antiphase boundary. We can assume that the actual TO_{2o} mode is shifted to lower frequencies and is buried inside the TO_2 band. Its shift toward the LO_2 band is not supported by the absence of the positive anisotropy at higher frequencies, however.

After the transition [Fig. 5(b)], the {110} anisotropy for the LO_1 and LO_2 band becomes positive in the 360–380 cm^{-1} region. This reflects the GaP-type character of these modes. In contrast the anisotropy of the TO_2 band reveals negative values, thus reflecting the InP-type LO mode contribution. This is what is expected for the unrelaxed model.[43] The 351-cm^{-1} peak conserves the positive anisotropy but becomes nearly two times weaker.[4]

We observed the reverse situation in a thin $GaInP_2$ layer (thickness 0.3 μm) with $\eta\sim0.5$[4] in which the initial state of the sample showed the unrelaxed type of {110} anisotropy similar to Fig. 5(b), while after cooling it became the relaxed type as shown in Fig. 5(a).[44]

We observed that the initial states of these samples can be restored after annealing.

The {110} anisotropy of the low ordered sample [Fig. 5(c)] clearly demonstrates the unrelaxed-type behavior with the negative contribution for the TO_2 band (LO InP type).

Summarizing our observations for the [001] backscattering geometry we can conclude that the martensitic transition occurs due to a switching of the ordered domains between relaxed and unrelaxed states and that the main driving force of the transition is the bond relaxation from ''zinc blende'' to ''trigonal'' atom positions. The trigonal relaxation becomes favorable with increasing ordering parameter and layer thickness, which is governed by the symmetry misfit strain. Thus in our thin sample the initial state is the unrelaxed state with the {110} anisotropic misfit strain below $\sim0.3\%$ as was discussed above. Rapid cooling of this sample causes a martensitic transition to the relaxed state, which has several times higher mismatch. In our thick sample symmetry misfit strain is relaxed and the initial and the martensitic states are reversed.

We should point out that the switching between the lattice states can be associated with the generation of the IR radiation, and it may therefore be possible to create strong lattice instability in $GaInP_2$ and generate infrared light using the martensitic transition.

TABLE III. Comparison of relative intensities of the TO_2 Raman band of spontaneously ordered $GaInP_2$ ($\eta \sim 0.5$) and the BPM selection rules for $[\bar{1}11]$ wave-vector configurations.

Geometry	Configuration	Selection rules		Relative intensity	Modes contributed
		TO	LO	(Ref. 11)	
$[\bar{1}11]$	$Z(XZ)X$	1	$2(1-\frac{2}{3}\Delta_\nu)^2$	0.7	$TO_\perp$
Right-angle	$Z(YY)X$	2	1	2	$TO_\perp$
Scattering	$Z(YZ)X$	3	0	3	$TO_\perp$
	$Z(XY)X$	0	0	$\ll 0.1$	
$[\bar{1}11]$	$z'(x'x')z'$	2	1	3	$TO_\perp + LO + Y'$
Backscattering	$z'(y'y')z'$	2	1	2.4	$TO_\perp + LO$
	$z'(y'x')z'$	2	0	2	$TO_\perp$

Our results show that one can distinguish between the unrelaxed and relaxed states in the Raman spectra by the magnitude of the InP-type LO or GaP-type mode contribution to the TO_2 band and by the intensity of the 351-cm^{-1} peak. Several unusual observations of the Raman activity of the TO_2 band and 351-cm^{-1} peak in different scattering geometries[11–13] can be interpreted in terms of the martensitic states. These observations also give evidence that not only thermal treatment but also a mechanical treatment arising from polishing or cleaving the sample can stimulate the martensitic transition.

2. Spectra for the wave vector $[\bar{1}11]$

Table III presents a comparison of the selection rules with experimental data for the TO_2 band for $[\bar{1}11]$ backscattering and right-angle scattering geometries from Ref.[11]. We can see that for the right-angle scattering geometry, involving (001) growth and (110) cleaved planes, the experimentally observed intensity distribution of (XZ), (YY), and (YZ) configurations (0.7, 2, and 3, respectively) agrees well with the TO mode character and manifests the relaxed state of the sample, which is consistent with the results for the [001] backscattering geometry. In contrast, for the backscattering geometry, in which the $(\bar{1}11)$ plane was prepared by mechanical polishing, the higher intensity of the TO_2 band in the diagonal configurations is a direct indication of the LO mode contribution and manifests the unrelaxed state of the sample. This gives evidence that the martensitic transition can be induced by mechanical polishing. It is also quite unusual that for this highly ordered sample the 351-cm^{-1} peak is absent in the spectra. On the other hand, there is an evident experimental intensity asymmetry of the TO_2 band in the diagonal configurations ($I_{x'x'} > I_{y'y'}$), which indicates the contribution of the $[\bar{1}10]$ polarized Y' mode (tensor 1b). As the 351-cm^{-1} peak also has $[\bar{1}10]$ polarization,[45] we can assume that due to a relaxation suppression the frequency of the corresponding mode shifted ~ 30 cm^{-1} to lower frequencies leading to a disappearance of the 351-cm^{-1} peak. This is not surprising in view of the strong $CuPt_B$ bond-relaxation-induced frequency shifts predicted by a first-principles model. Such a shift can explain decrease by a factor of 2 of the intensity of the 351-cm^{-1} peak in [001] backscattering spectra in Fig. 5(b). The fact that this peak does not disappear after transition indicates coexistence of relaxed and unrelaxed states of the sample in Fig. 5(b).

3. Spectra for the wave vector [110]

Analysis of the intensities of the TO_2 band (I_{TO_2}) and 351-cm^{-1} peak ($I_{Y'}$) in $x'z'$, $x'x'$, and $z'z'$ configuration from Refs. 11 and 13, summarized in Table IV, allows us to demonstrate the existence of the differently relaxed states in the [110] backscattering geometry, which involves the (110) cleaved plane. In Ref. 11 for $I_{TO_2}:I_{Y'} \sim 7$ the intensity ratio $I_{x'z'}:I_{x'x'}:I_{z'z'}$ is 1:2:3, while in Ref. 13 for $I_{TO_2}:I_{Y'} \sim 17$ it is 1:8:4. As can be seen from the selection rules presented in

TABLE IV. The BMP selection rules and relative Raman intensities of the TO_2 band of $GaInP_2$ ($\eta \sim 0.5$) for [110] wave-vector scattering configurations.

Configuration			TO_2 band Experiment (Ref. 11) ($I_{TO_2}:I_{Y'} \sim 7$)		Experiment (Ref. 13) ($I_{TO_2}:I_{Y'} \sim 17$)	
	$TO\parallel$	$TO\perp$	Relative intensity	Modes contribution	Relative intensity	Modes contribution
$y'(z'z')\bar{y}'$	$4(1-\Delta_\nu)^2$	0	3	$TO_\parallel$	4	$TO_\parallel$
$y'(x'x')\bar{y}'$	1	2	2	$TO_\perp + TO_\parallel$	8	$TO_\perp + TO_\parallel$
$y'(x'z')\bar{y}'$	0	1	1	$TO_\perp$	1	$TO_\perp$

Table IV, both of the ratios strongly differ from the ratio 1:3:4 expected for $\Delta_\nu \sim 0$ and for isotropic contribution of the modes polarized along ($TO_\parallel$) and perpendicular to the ($TO_\perp$) ordering direction. The intensity ratio 1:2:3 observed in Ref. 11 implies a very small contribution of the $TO_\parallel$ (extraordinary) modes ($I_{TO\parallel x'x'} \gg I_{TO\perp x'x'}$) and their GaP-type character ($\Delta_\nu < 0$ for $I_{TO\parallel z'z'} > I_{TO\parallel x'x'}$). This indicates the relaxed state. In contrast the ratio 1:8:4 implies dominance of the contribution of the $TO_\parallel$ extraordinary modes ($I_{TO\parallel x'x'} \gg I_{TO\perp x'x'}$) and their InP-type character ($1 > \Delta_\nu > 0.5$ for $I_{TO\parallel z'z'} > I_{TO\parallel x'x'}$). This indicates the unrelaxed state and correlates with a much smaller ($\sim \frac{1}{17}$) relative intensity of the 351-cm^{-1} mode. These results give evidence on the possibility of triggering the martensitic transition by the cleaving procedure.

It should be noted that the strong asymmetry of the $TO_\parallel$ and $TO_\perp$ contributions (difference in vibrational amplitudes) is not predicted by the lattice dynamical calculations and demonstrates a very complicated behavior of the phonon modes in the spontaneously ordered $GaInP_2$, which can be associated with the antiphase boundaries (APB's). Due to its nature (boundary between domains) the APB's determine boundary conditions for vibrational modes of the ordered domains. We can assume that the APB's can produce phase shifts of atom vibrational amplitudes in the adjacent domains, leading to constructive/destructive interference effects in the intensity of the corresponding modes.

B. The antiphase boundaries in the Raman spectra of spontaneously ordered $GaInP_2$

The existence of the antiphase boundaries in spontaneously ordered $GaInP_2$ is well documented by a large set of transmission electron microscopy (TEM) measurements.[46–51]. In dark-field [110] cross-section TEM images taken using ordering-induced diffraction spots, the APB's appear as (1–40)-nm-wide dark contrast lines separating bright contrast ordered domains having sizes 5–500 nm. The dark contrast appears due to destructive interference between the diffracted beams from the adjacent domains, which confirm the fact that the lines originate from the APB's rather than from a disordered material. The APB's generally propagate from the substrate/epilayer interface to the top surface at an angle to the (001) plane, and occupy up to ~10% of the total area. The structural diagram of an atomically sharp antiphase domain boundary for the $[\bar{1}11]$ variant $GaInP_2$ presented in Fig. 6 shows that it consists of $[\bar{1}10]$ and $[\bar{1}11]$ interfaces. The $[\bar{1}10]$ interface can be considered as a thin layer of a $[1\bar{1}1]$ variant and the $[\bar{1}11]$ interface consists of a $[\bar{1}11]$ InP (GaP) bilayer. According to the TEM images taken with atomic resolution, the APB's are usually not so sharp and occupy several monolayers.[46–48] This is schematically shown in Fig. 6 as intermixing of In and Ga atom sites which leads to the formation of $[\bar{1}10]$ InP and GaP chains inside the APB.

As the APB's occupy a relatively large amount of epilayer volume they must have a strong effect on the optical properties of spontaneously ordered $GaInP_2$. Indeed, they appeared

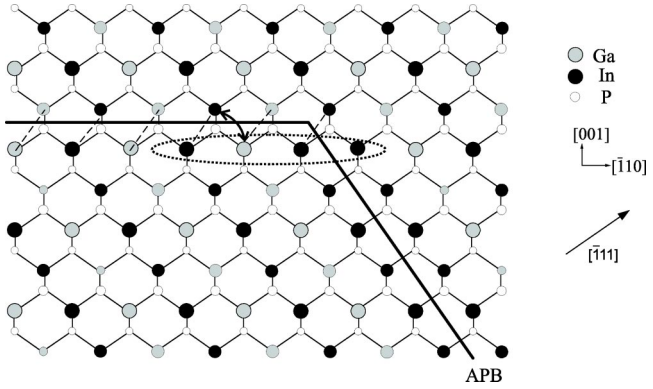

FIG. 6. Atom arrangement of an atomically sharp antiphase boundary (APB) in the $[\bar{1}11]$ variant $CuPt_B$ $GaInP_2$. Gray, black, and open circles denote Ga, In, and P atoms, respectively. Smaller symbols correspond to a next-lower-lying layer; dashed lines link APB atoms creating the $[1\bar{1}1]$ variant; dashed oval outlines the $[\bar{1}10]$ InP chain which forms by interchanging of Ga and In atom positions linked by arrow (boundary diffusing).

in low-temperature photoluminescence as ultranarrow sharp lines, which reflect strong, quantum-dot-like confinement of an exciton at APB's.[51,52] In vibrational spectra the APB can be associated with the 351-cm^{-1} peak.

The 351-cm^{-1} peak in earlier studies was interpreted in terms of the lattice dynamics of the perfectly ordered structure and was assigned to either a TO (Refs. 4, 10, and 14) or an LO mode of $CuPt_B$ $GaInP_2$ structure.[9,11,12,14] Its interpretation as a TO mode was based on its $[\bar{1}10]$ polarization for the [001] backscattering geometry as described above,[4] while its interpretation as an LO mode was based mainly on the fact that this peak was unresolved in the LO forbidden [110] geometry in earlier studies.[11,12] Recent analysis of the activity of this peak in the $[\bar{1}11]$ right-angle and [110] backscattering configurations also shows its $[\bar{1}10]$ polarization, i.e., its Y' mode origin.[45] This directly follows from the dominance of the 351-cm^{-1} peak in $Z(XZ)X$ and $y'(x'x')y'$ configurations for the $[\bar{1}11]$ right-angle and [110] back scattering geometries, respectively (Table I). Comparison of the experimental data[11,13] with the selection rules for the [110] geometry presented in Table V shows the InP-type character of this mode. Indeed, experimentally ob-

TABLE V. The BPM selection rules and relative Raman intensities of the 351-cm^{-1} peak of $GaInP_2$ ($\eta \sim 0.5$) for [110] wavevector scattering configurations.

Configuration	351-cm^{-1} peak		
	Y'	Experiment (Ref. 11)	Experiment (Ref. 13)
$y'(z'z')y'$	$\frac{8}{3}(1-\Delta_\nu)^2$	~0.3	<0.1
$y'(x'x')y'$	$\frac{8}{3}$	1	1
$y'(x'z')y'$	$\frac{1}{3}$	~0.1	<0.1

[a]We present here an estimation of the intensity of the group of overlapping peaks centered at ~360 cm^{-1}.[45]

served suppression of this mode in the $(z'z')$ configuration agrees well with the selection rules for the Y' mode, under the condition $1>\Delta_\nu>0$. This condition can be satisfied only for the InP-type modes. The very low relative $(z'z')$ intensity (~ 0.3 and >0.1) indicates its strong localization ($U_2^I = 0$) (Table II).

As the direction of the $[\bar{1}10]$ polarization does not coincide with the crystal axis of the $CuPt_B$ structure, the activation of the Y' mode in the $[\bar{1}11]$ and [110] wave-vector geometries cannot be related to the $CuPt_B$ order. The $[\bar{1}10]$ polarization gives evidence of the APB origin of the 351-cm^{-1} peak. Independence of the polarization on the wave vector shows the strongly localized nature of this vibration. We can assume that the Y' mode corresponds to the vibrations of $[\bar{1}10]$ InP chains formed inside the diffuse APB (Fig. 6). In the martensitic transition the frequency of the APB mode switches between 351-cm^{-1} (relaxed state) and 330-cm^{-1} (unrelaxed state) leading to a correlation between intensities of the 351-cm^{-1} peak and the TO_2 band.

IV. CONCLUSIONS

In conclusion we have shown that the martensitic transition in epitaxial layers of spontaneously ordered $GaInP_2$ originates from the relaxation of bonds in the $CuPt_B$ atomic arrangement. This is revealed in the Raman spectra due to a strong effect of the bond relaxation on the phonon properties of $CuPt_B$-ordered $GaInP_2$, and due to specific selection rules of this structure which allow one to distinguish the modes of different sublattices. This was demonstrated in two ways: first, by comparison of the shell-model lattice dynamical calculations (using zinc-blende bond lengths and interatomic potentials) from our previous study[4] and by the first-principles lattice dynamical calculations from Ref. 24. Second, it was demonstrated by using the bond polarizability model of CuPt $GaInP_2$ described in Refs. 4 and 29. We used the Raman selection rules obtained in the bond polarizability model to analyze the experimental intensity of optical-phonon bands in spontaneously ordered $GaInP_2$ for (001) growth[4] and from (110) cleaved and $(\bar{1}11)$ polished[11–13] excitation planes. Our analysis shows that thermal treatment-induced changes (martensitic transition) of the {110} diagonal anisotropy of LO_1, LO_2, TO_2 phonons and the 351-cm^{-1} mode observed in Ref. 4 are driven by the bond relaxation and symmetry misfit strains. The evidence that the martensitic transition and lattice relaxation in $GaInP_2$ can be induced by mechanical treatment is found from the analysis of the intensities of the 351-cm^{-1} peak and TO_2 band for excitation using cleaved and polished planes. Our analysis allows us to assign the 351-cm^{-1} mode to the vibration of the [110] InP chains of an antiphase boundary, and allows us to show that in the martensitic transition the frequency of this mode switches between 351-cm^{-1} (relaxed state) and 330 cm^{-1} (unrelaxed state). We demonstrate extremely high sensitivity of Raman spectroscopy to changes of atomic arrangement due to the martensitic transition in semiconductor alloys.

ACKNOWLEDGMENTS

The authors wish to thank the W. M. Keck Foundation and the DARPA/ONR Grant No. N00014-01-1-0658 for support.

[1] A. Zunger and S. Mahajan, *Handbook on Semiconductors* (Elsevier, Amsterdam, 1994), Vol. 3.

[2] An-Ban Chen and Arden Sher, *Semiconductor Alloys, Physics and Material Engineering* (Plenum Press, New York, 1995) p. 349.

[3] *Compositional Modulation and Spontaneous Ordering in Semiconductors*, edited by T.P. Persal and G.B. Stringfellow [MRS Bull. **22**, 7 (1997)].

[4] A.M. Mintairov, J.L. Merz, A.S. Vlasov, and D.V. Vinokurov, Semicond. Sci. Technol. **13**, 1140 (1998).

[5] A.G. Khachaturyan, *Theory of Structural Transformations in Solids* (Wiley, New York, 1983).

[6] M. Kondow and S. Minagawa, J. Appl. Phys. **64**, 793 (1988).

[7] K. Uchida, P.Y. Yu, N. Noto, Z.-L. Weber, and E.R. Weber, Philos. Mag. B **70**, 453 (1994).

[8] A. Gomyo, T. Suzuki, K. Kobayashi, S. Kawata, I. Hino, and T. Yuasa, Appl. Phys. Lett. **50**, 673 (1987).

[9] F. Alsina, N. Mestres, J. Pascual, C. Geng, P. Ernst, and F. Scholz, Phys. Rev. B **53**, 12 994 (1996).

[10] A.M. Mintairov and V.G. Melehin, Semicond. Sci. Technol. **11**, 904 (1996).

[11] H.M. Cheong, F. Alsina, A. Mascarenhas, J. Geisz, and J.M. Olson, Phys. Rev. B **56**, 1888 (1997).

[12] N. Mestres, F. Alsina, J. Pascual, J.M. Bluet, J. Camassel, C. Geng, and F. Scholz, Phys. Rev. B **54**, 17 754 (1996).

[13] M.J. Seong, A. Mascarenhas, J.M. Olson, and H.M. Cheong, Phys. Rev. B **63**, 235205 (2001).

[14] A. Hassine, J. Sapriel, P. Le-Berre, M. A. Di-Forte-Poisson, F. Alexandre, and M. Quillec, Phys. Rev. B **54**, 2728 (1996).

[15] A.M. Mintairov, B.N. Zvonkov, T.S. Babushkina, I.G. Malkina, and Yu.N. Saf'yanov, Solid State Phys. **37**, 3607 (1995).

[16] H.M. Cheong, A. Mascarenhas, P. Ernst, and C. Geng, Phys. Rev. B **56**, 1882 (1997).

[17] H.M. Cheong, A. Mascarenhas, J.F. Geisz, and J.M. Olson, Phys. Rev. B **62**, 1536 (2000).

[18] K. Sinha, A. Mascarenhas, G.S. Horner, R.G. Alonso, K.A. Bertness, and J.M. Olson, Phys. Rev. B **48**, 17 591 (1993).

[19] K. Sinha, A. Mascarenhas, G.S. Horner, K.A. Bertness, S.R. Kurtz, and J.M. Olson, Phys. Rev. B **50**, 7509 (1994).

[20] A. Krost, N. Esser, H. Selber, J. Christen, W. Richter, D. Bimberg, L.C. Su, and G.B. Stringfellow, J. Cryst. Growth **145**, 171 (1994).

[21] A. Krost, N. Esser, H. Selber, J. Christen, W. Richter, D. Bimberg, L.C. Su, and G.B. Stringfellow, J. Vac. Sci. Technol. B **12**, 2558 (1994).

[22] Y. Zhang and A. Mascarenhas, J. Raman Spectrosc. **32**, 831 (2001).

[23] V. Ozolins and A. Zunger, Phys. Rev. B **57**, R9404 (1998).
[24] V. Ozolins and A. Zunger, Phys. Rev. B **63**, 087202 (2001).
[25] F. Alsina, N. Mestres, A. Nakhli, and J. Pascual, Phys. Status Solidi B **215**, 121 (1999).
[26] F. Alsina, H.M. Ceeong, J.D. Webb, A. Mascarenhas, J.F. Geisz, and J.M. Olson, Phys. Rev. B **56**, 13 126 (1997).
[27] F. Alsina, J.D. Webb, A. Mascarenhas, J.F. Geisz, J.M. Olson, and A. Duda, Phys. Rev. B **60**, 1484 (1999).
[28] T. Hofmann, V. Gottschalch, and M. Schubert, Phys. Rev. B **66**, 195204 (2002)
[29] A. Mascarenhas, H.M. Cheong, F. Alsina, J.F. Geisz, and J.M. Olson, Phys. Rev. B **63**, 247202 (2001).
[30] P.H. Borcherds, G.F. Alfrey, D.H. Saunderson, and A.D.B. Woods, J. Phys. C **8**, 2022 (1975).
[31] P.H. Borcherds, K. Kunc, G.F. Alfreys, and R.H. Hall, J. Phys. C **12**, 4699 (1979).
[32] To distinguish GaP- and InP-type modes in ordered structure in Fig. 2 we assign P atoms of triple bonds as atoms belonging to a corresponding monolayer. Accordingly, we labeled the mode in which these atoms have their largest displacement by the type of triple bond. Thus the displacement of the P1 atom corresponds to the InP-type phonon and the displacement of the P2 atom to the GaP-type phonon [inset in Fig. 1(a)]. We used subscript 1 for the GaP-type modes and 2 for the InP-type ones. This differs from notations of Ref. 24.
[33] For illustration purposes we neglect angular anisotropy and used frequency values averaged between ordinary and extraordinary mode frequencies. For phonon damping we used values from Fig. 2.
[34] We used values obtained from our unpublished IR reflectivity spectra.
[35] A.M. Mintairov, N.A. Sadchikov, T. Sauncy, M. Holtz, G.A. Seryogin, S.A. Nikishin, and H. Temkin, Phys. Rev. B **59**, 15 197 (1999).
[36] D.B. Laks, S.-H. Wei, and A. Zunger, Phys. Rev. Lett. **69**, 3766 (1992).
[37] R. Loudon, Adv. Phys. **13**, 423 (1964).
[38] M.L. Faust and C.R. Henry, Phys. Rev. Lett. **17**, 1265 (1966).
[39] M. Wolkenstein, Dokl. Akad. Nauk **30**, 791 (1941).
[40] R. Tubino and L. Piseri, Phys. Rev. B **11**, 5145 (1973).
[41] B. Jusserand and M. Cardona, in *Light Scattering in Solids V*, edited by M. Cardona and G. Guntherodt (Springer, Berlin, 1989), p. 91.
[42] M.I. Alonso, P. Castrillo, G. Armelles, A. Ruiz, M. Recio, and F. Briones, Phys. Rev. B **45**, 9054 (1992).
[43] The appearance of the LO InP-type contribution at frequency $\sim 330\ \mathrm{cm}^{-1}$, which is lower than predicted by this model could be due to the partial character of the ordering. However, frequency $330\ \mathrm{cm}^{-1}$ coincides with the *L* boundary phonon frequency of bulk InP (Fig. 2).
[44] It should be noted that in the relaxed state of both samples our Lorentzian decomposition reveals InP-type negative anisotropy of weak mode at $340\mathrm{cm}^{-1}$ (see also Ref. 28). This mode can be assigned as arising from unrelaxed $GaInP_2$ and demonstrates the possible coexistence of relaxed and unrelaxed phases.
[45] A.M. Mintairov, J.L. Merz, and A.S. Vlasov, Phys. Rev. B **63**, 247201 (2001).
[46] O. Ueda, M. Takikawa, M. Takechi, J. Komeno, and I. Umebu, J. Cryst. Growth **93**, 418 (1988).
[47] C.S. Baxter, W.M. Stobbs, and J.H. Wilkie, J. Cryst. Growth **112**, 373 (1991).
[48] L.C. Lu, I.H. Ho, and G.B. Stringfellow, J. Appl. Phys. **75**, 5135 (1994).
[49] P. Ernst, C. Geng, G. Hahn, F. Scholz, H. Schweizer, F. Phillipp, and A. Mascarenhas, J. Appl. Phys. **79**, 2633 (1996).
[50] H.M. Cheong, A. Mascarenhas, S.P. Ahrenkiel, K.M. Jones, J.F. Geisz, and J.M. Olson, J. Appl. Phys. **83**, 5418 (1998).
[51] U. Kops, P.G. Blome, M. Wenderoth, R.G. Ulbrich, C. Geng, and F. Scholz, Phys. Rev. B **61**, 1992 (2000).
[52] H.M. Cheong, A. Mascarenhas, J.F. Geisz, J.M. Olson, M.W. Keller, and J.R. Wendt, Phys. Rev. B **57**, R9400 (1998).